Journal of Applied Polymer Science

Multifunctional Polyaniline–Tin Oxide (PANI–SnO_2) Nanocomposite: Synthesis, Electrochemical, and Field Emission Investigations

Sandip S. Patil,[1] Kashmira V. Harpale,[2] Shankar P. Koiry,[3] Kashinath R. Patil,[4] Dinesh K. Aswal,[3] Mahendra A. More[2]

[1]Department of Physics, Modern College of Arts, Science and Commerce, Shivaji Nagar, Pune 411005, India

[2]Center for Advanced Studies in Material Science and Condensed Matter of Physics, Department of Physics, Savitribai Phule Pune University, Pune 411007, India

[3]Technical Physics Division, Bhabha Atomic Research Center, Trombay, Mumbai 400 085, India

[4]National Chemical Laboratory (NCL), Council of Scientific and Industrial Research (CSIR), Dr. Homi Bhabha Road, Pune 411008, India

Correspondence to: M. A. More (E-mail: mam@physics.unipune.ac.in) and S. S. Patil (E-mail: sandippatil1712@gmail.com)

ABSTRACT: Synthesis of PANI–SnO_2 nanocomposite has been performed using a simple two step chemical oxidative polymerization route. The structural, morphological and chemical properties of the as-synthesized PANI–SnO_2 nanocomposite have been revealed by various characterization techniques such as SEM, TEM, XRD, FTIR, and XPS. Interestingly the as-synthesized PANI–SnO_2 nanocomposite exhibits supercapacitance value of 721 F g^{-1} with energy density 64 Wh kg^{-1}, which is noticed to be higher than that of pristine SnO_2 and PANI nanostructures. Furthermore, the galvanostatic charge–discharge characteristics revealed pseudocapacitive nature of the PANI–SnO_2 nanocomposite. The estimated values of charge transfer resistance and series resistance estimated from the Nyquist plot are found to be lower. Along with the supercapacitive nature, PANI–SnO_2 nanocomposite showed promising field emission behavior. The threshold field, required to draw emission current density of 1 $\mu A/cm^2$, is observed to be 0.90 V/μm and emission current density of 1.2 mA/cm^2 has been drawn at applied field of ~2.6 V/μm. The emission current stability investigated at preset values of 0.02 and 0.1 mA/cm^2 is observed to be fairly stable over duration of more than 3 h. The enhanced supercapacitance values, as well as, the promising field emission characteristics are attributed to the synergic effect of SnO_2 nanoparticles and PANI nanotubes. © 2014 Wiley Periodicals, Inc. J. Appl. Polym. Sci. **2015**, *132*, 41401.

KEYWORDS: conducting polymers; electrochemistry; nanostructured polymers; surfaces and interfaces

Received 2 June 2014; accepted 18 August 2014
DOI: 10.1002/app.41401

INTRODUCTION

Polyaniline (PANI) has received a great deal of attention as one of the materials of choice for frontline multidisciplinary research areas, because of its inherent superior physico-chemical properties.[1–3] The domain of applications of PANI, its nanostructures and nanocomposites is quite wide, which includes chemical sensors, battery electrodes, corrosion inhibition, electromagnetic interference shielding, light emitting diodes, solar cells, supercapacitors and field emission (FE).[1,3] In recent years, electrochemical supercapacitors are being considered as potential energy efficient devices facilitating rapid energy storage and delivery. The supercapacitors offer unprecedented advantages such as, high power density, high efficiency, long life cycle, stable performance over wide range of operational temperature, and eco-friendly nature.[4] Owing to these advantages, they show potential for practical applications in variety of portable devices like digital cameras, mobile phones, in addition to hybrid vehicles and energy storage units for solar cells. However, certain issues dealing with energy density, self charging rate, cost etc, limit their real field applications on massive scale, and therefore there is need of more research to overcome these limitations.

As the performance of supercapacitors critically depends on the nature of electrolyte and electrode material, conducting polymers and nanostructured metal oxides exhibiting psuedocapacitance behavior are considered to be promising electrode materials. Moreover, PANI, due to its fast redox switching and excellent energy storage capacity, is recognized as an ideal electrode material for supercapacitors.[5] As a consequence, a good amount of research work exploring various PANI nanostructures (nanowires, nanobuds, hollow nanofibers etc.) for supercapacitive application has been reported in the last couple of years.[6–8] Although, the PANI nanostructures exhibit high capacitance, it is seen that the polymer

backbone break down occurs after limited charging–discharging cycles. The poor strength and modest rigidity of the polymer backbone leads to reduced cycling stability.[9] This limitation can be overcome, if sufficient strength to the polymer backbone is provided, which can be achieved via use of PANI nanocomposites.[10] In this regard, Kovalenko et al. have investigated the supercapacitive behavior of PANI-nanodiamond composite. The authors have observed that, incorporation of nanodiamond in PANI matrix increases the performance of electrochemical supercapacitor, and with the increase in percentage of nanodiamond noticeable improvement in cycle stability and retention in capacitance value, as compared to pristine PANI is observed.[10] Some research groups have investigated various nanocomposites of PANI with graphene, carbon fibers, single walled carbon nanotubes, reduced graphene oxide (RGO), graphite nanofibers, and have observed enhanced supercapacitance values with better stability.[5,9,11–17] Besides nanocomposites of PANI with carbon based materials, nanocomposites of metal oxides and carbon family members such as, SnO_2@C, SnO_2/graphene, MnO_2/graphene, RuO_2/graphene, RGO/MoO_3, etc. have been studied as supercapcitors.[18–20] Recently, Zhu et al. and Wang et al. reported the supercapacitive investigations of PANI–SnO_2 nanocomposite, wherein they have found the highest supercapacitance 857 F g^{-1} and 335.5 F g^{-1}, respectively.[21,22] There are a few more groups which have studied the supercapacitive behavior of PANI–SnO_2 hybrid structures.[23,24]

In addition to the supercapacitive performance of the PANI nanostructures and nanocomposites, their field electron emission characteristics are observed to be interesting and thus, have been investigated by various research groups.[25–30] Recently, our group has reported FE properties of various nanostructures of PANI such as nanotubes, nanofibers, nanopetals, and nanocrystals.[31–33]

Amongst the various PANI-metal oxide nanocomposites, the PANI–SnO_2 is an interesting system possessing a unique set of properties owing to superior intrinsic properties of the counterparts.[34,35] We herein, report synthesis of PANI–SnO_2 nanocomposite and its multifunctionality in terms of electrochemical supercapacitance and FE behavior. The structural and chemical characterization of the PANI–SnO_2 nanocomposite was carried out using scanning electron microscope (SEM), transmission electron microscope (TEM), X-ray diffraction (XRD), Fourier transform infrared spectroscopy (FTIR), and X-ray photoelectron spectroscopy (XPS). The electrochemical properties pertaining to the supercapacitive behavior were investigated employing cyclic voltammetry (CV), galvanostatic charge–discharge (GCD), and electrochemical impedance spectroscopy (EIS) techniques.

EXPERIMENTAL

The PANI–SnO_2 nanocomposite was synthesized in two steps. In the first step, SnO_2 nanoparticles were synthesized by chemical route in separate experiment, and in the second step, these nanoparticles were used to synthesize the PANI–SnO_2 nanocomposite during oxidative polymerization of PANI.

Materials

The source chemicals such as aniline monomer (C_6H_7N), acetic acid (CH_3COOH) and sulfuric acid (H_2SO_4) were obtained from Central Drug House LTD, New Delhi, India, while tin chloride [$SnCl_4{\cdot}5H_2O$ (A.R.)], liquid ammonia (NH_3) and ammonium persulphate (APS) [$(NH_4)_2S_2O_8$] were purchased from Thomas Baker, Mumbai, India.

SnO_2 Nanoparticle Synthesis

The synthesis of SnO_2 nanoparticles was carried out by a facile sol–gel route, wherein 2*M* liquid NH_3 was drop wise added to 0.2*M* aqueous solution of $SnCl_4{\cdot}5H_2O$. The slow addition liquid NH_3 converts the stannic chloride solution into opal gel, which was collected and washed with distilled water several times. The gel was then centrifuged to remove excess water and chlorine, and the precipitate was dried at 80°C. The resultant SnO_2 powder was annealed at 500°C for 5 h in ambient.[36]

PANI–SnO_2 Nanocomposite Synthesis

To synthesize the nanocomposite, the SnO_2 nanoparticles were added during polymerization of PANI. First, 0.25*M* APS was slowly added to the mixture of 0.2*M* double distilled aniline and 0.8*M* acetic acid.[31] Upon addition of APS followed by continuous stirring the reaction mixture turned from colorless to brown, and finally to dark green. At this stage, the SnO_2 nanoparticles were added to the reaction mixture and kept at static condition for 24 h. Next day the solution was filtered and washed several times with double distilled water and ethanol. The filtered residue was dried at 60°C under rough vacuum conditions. The synthesis process can be summarized as below.

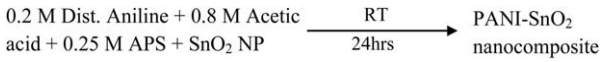

Characterization

The synthesized nanocomposite was characterized by Scanning Electron Microscope (SEM, Model—JEOL, JSM 6360A), Transmission Electron Microscope (TEM, Model—FEI, Technai G^2 U20) and X-Ray Diffractometer (XRD, Model—D8, Advance, Bruker AXS) so as to reveal its structural and morphological properties. The chemical properties were studied by Fourier Transform Infrared Spectrometer (FTIR, Model—JASCO, 6100). The XPS analysis was carried out at the base pressure of 10^{-10} mbar, using Mg K_α radiation (1253.6 eV, line width 0.7 eV) generated at a power of 150 W using X-ray photoelectron spectrometer (XPS, VG Microtech ESCA 3000).

Preparation of Working Electrodes and Electrochemical Measurements

The electrochemical measurements were performed using three electrode assembly in single compartment glass cell wherein platinum foil and saturated calomel electrode (SCE) were used as counter and reference electrodes, respectively. The working electrode was prepared by drop casting the electrode material on the indium doped tin oxide (ITO, conductivity $\sim$ 0.5 Ω cm^{-1}) glass substrate. The weight of the ITO glass was taken before and after the drop casting in order to calculate mass of the electrode material. Separate working electrodes were prepared for SnO_2 nanoparticles, PANI nanotubes, and PANI–SnO_2 nanocomposite. A computer interfaced electrochemical analyzer (1100A Series, CH Instrument) has been used to carry out electrochemical measurements of these working electrodes, one at a time. The CV measurements were performed in 1*M* H_2SO_4 electrolyte by sweeping the potential between −0.2 and

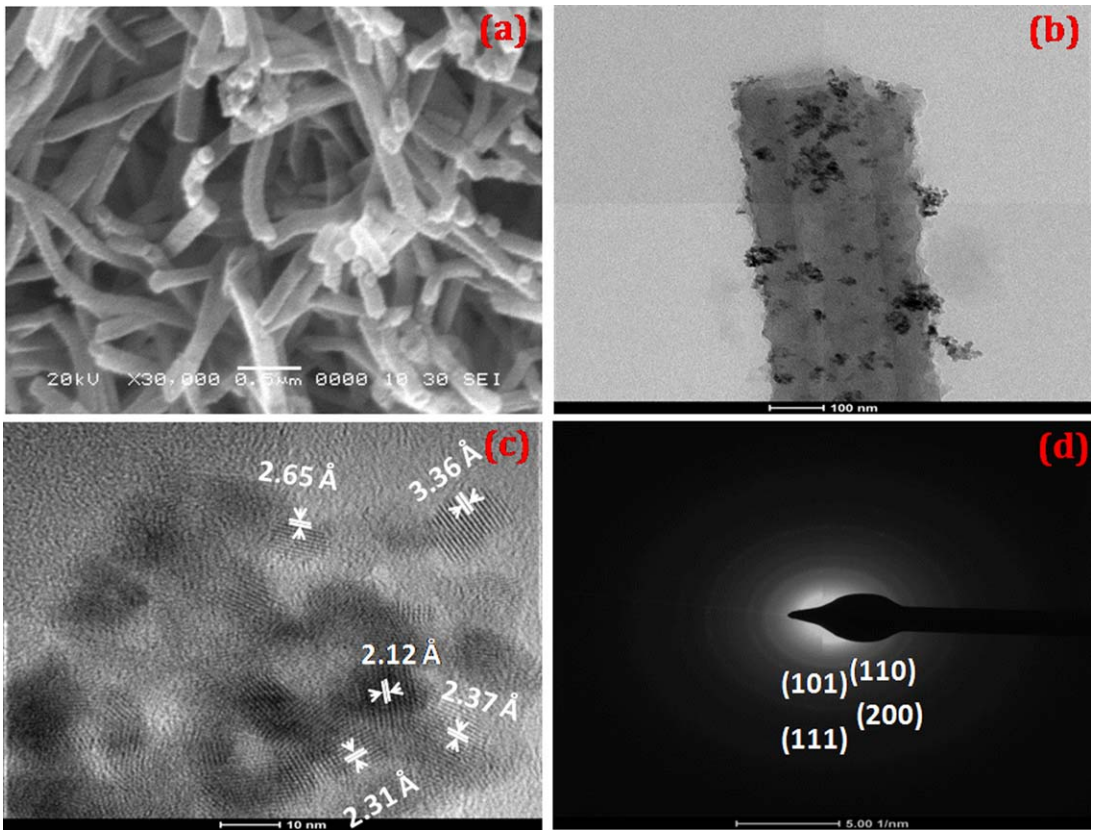

Figure 1. (a) SEM image, (b) TEM image, (c) High resolution TEM image, and (d) SAED pattern of the PANI–SnO_2 nanocomposite. [Color figure can be viewed in the online issue, which is available at wileyonlinelibrary.com.]

0.8 V at different scan rates, ranging from 0.005 to 0.5 V/s. The specific capacitance (C_{sp}) of the nanocomposite is calculated by the formula:

$$C_{sp} = \frac{I}{m.s}$$

where, I is the peak current, m is the mass of electrode material, and s is the scan rate. Furthermore, the maximum energy storage (E) per unit mass i.e. energy density has been calculated using following formula,

$$E = \frac{1}{2} C_{sp} V_i^2$$

where, V_i is the initial voltage of the discharge curves.

The charging–discharging studies of the PANI–SnO_2 nanocomposite electrode were carried out at different current values 9, 8, 7, 5, and 4 A g^{-1} and from the galvanostatic discharge curves, the specific capacitance was calculated as per the following formula,

$$C_{sp} = \frac{2 \times I}{m.(\Delta V/\Delta t)}$$

where "I" is discharging current, "m" is mass of active electrode material, and "$(\Delta V/\Delta t)$" is the average slope of discharge curve. Furthermore, the impedance spectroscopy measurements were performed in the frequency range from 100 MHz to 1 mHz using FRA2 Autolab workstation (Type III).

Field Emission Measurements

The FE measurements were carried out using a planar diode configuration at base pressure of $\sim 1 \times 10^{-8}$ mbar. The PANI–SnO_2 nanocomposite drop casted on copper stub acted as a cathode, whereas a semitransparent phosphor screen held parallel with the cathode acted as an anode. A linear motion drive facilitated variation in distance between the anode and cathode. In the present studies, the distance between anode and cathode was kept ~1 mm. The FE current versus voltage (I − V) and current versus time (I − t) measurements were carried out using Spellman high voltage DC power supply (±40 kV) and Kiethely 6514 Picoammeter. A special care was taken for low noise measurements and proper grounding. The details of vacuum processing and FE measurements are described elsewhere.[31]

RESULTS AND DISCUSSION

The SEM image [Figure 1(a)] of as-synthesized PANI–SnO_2 nanocomposite shows formation of PANI nanorods having diameter in the range from 200 to 300 nm, and length of several microns. A careful observation of SEM image reveals presence of agglomerates of tiny nanoparticles on surface of the PANI nanorods. To gain better structural understanding of these nanostructures, TEM analysis was performed. A typical TEM image of a single PANI nanostructure, depicted in Figure 1(b), reveals that the nanorod is hollow with inner cavity diameter of ~50 nm. From the TEM analysis, average size of the SnO_2

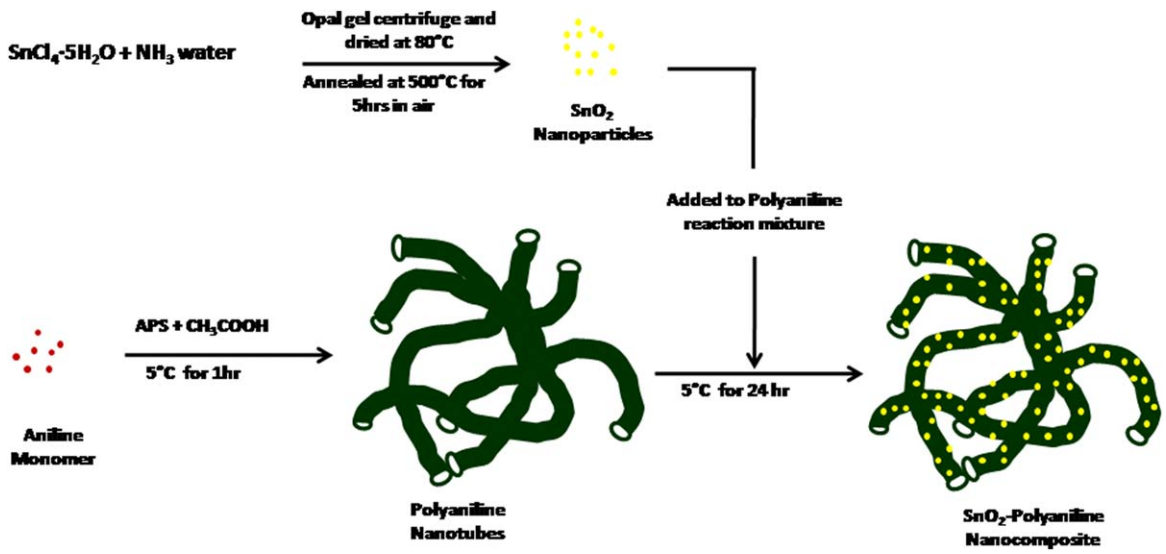

Scheme 1. Formation PANI–SnO_2 nanocomposite. [Color figure can be viewed in the online issue, which is available at wileyonlinelibrary.com.]

nanoparticles is estimated to be ~20 nm. The HRTEM image [Figure 1(c)] shows lattice fringes justifying crystalline nature of the SnO_2 nanoparticles, supported by the selected area electron diffraction (SAED) pattern [Figure 1(d)]. The observed SAED pattern, comprised of concentric rings suggests polycrystalline nature of the PANI–SnO_2 nanocomposite. The four bright rings implying interplanar spacing (d) values ~3.36, 2.65, 2.37, and 2.31 Å are representative of the (110), (101), (200), and (111) planes of SnO_2, respectively. Thus, the TEM analysis reveals that the nanocomposite is comprised of well adhered crystalline SnO_2 nanoparticles present on surface of the PANI nanotubes. The synthesis protocol of SnO_2 nanoparticles, PANI nanotubes, and PANI–SnO_2 nanocomposite is pictorially depicted in Scheme 1.

The EDAX spectrum [Figure 2(a)] recorded during the TEM analysis exhibits peaks related to Sn and O, confirming that the agglomorated nanoparticles are of SnO_2 phase. The other peaks representative of C and S due to PANI and oxidant (APS), respectively. For verification of the SnO_2 phase, XRD analysis was performed. A typical XRD pattern of the PANI–SnO_2 nanocomposite, shown in Figure 2(b), exhibits a set of well defined diffraction peaks. The diffraction peaks observed at different 2θ values; 26.4, 33.7, 37.8, 38.8, 51.5, 54.5, 61.6, 64.4, 65.7, 70.9, and 78.3, are indexed to (110), (101), (200), (111), (211), (220), (310), (112), (301), (202), and (321) planes of SnO_2, respectively (Ref JCPDS card # 770452). Thus, the XRD analysis indicates presence of polycrystalline SnO_2 nanoparticles having tetragonal phase in the composite films. The formation of conducting phase of PANI in the nanocomposite was revealed by UV–Visible spectrum shown in Figure 2(c).

The FTIR spectrum of PANI–SnO_2 nanocomposite is depicted in Figure 2(d), which is in good agreement with the earlier reports.[37–43] The peaks observed at ~1576 and 1508 cm^{-1} are due to the C═C stretching deformation of the quinoid and benzoid rings, respectively. The peaks observed at ~1302 and 1250 cm^{-1} are attributed to C—N stretching of secondary amines. Absorption due to attachment of $-SO_3^-$ group to the aromatic rings is indicated by the peaks at ~1040, and 695 cm^{-1}. The peaks present at 1177 and 826 cm^{-1} belong to the degree of delocalization of electron and out of plane vibration of C—H, respectively.[37–43]

The deconvoluted XPS spectra of the PANI–SnO_2 nanocomposite corresponding to C_{1s}, N_{1s}, O_{1s}, and Sn_{3d} energy levels are depicted in the Figure 3. The C_{1s} energy spectrum can is deconvoluted into three peaks at 284.6, 285.5, and 287.1 eV, as seen in Figure 3(a). The peak located at 284.6 eV is associated to the C—C bonding of sp^2 carbon (C_1). Furthermore, the peak observed at binding energy of ~285.5 eV (C_3) is associated to the C—N or C═N bonding, while the peak at ~287.1 eV (C_2) is due to the C—N^+ bond.[44] As seen from Figure 3(b), the deconvoluted XPS spectrum of N_{1s} energy level exhibits four peaks. The peaks corresponding to the binding energies 399.5 (N_1) and 400.33 eV (N_4) are attributed to the quinoid imine [═N—] and the benzoid imine [—NH—] bonds, respectively. In addition, the peaks observed at 400.52 (N_2) and 402.39 eV (N_3) are assigned to the cationic nitrogen atoms (═NH^+) and the protonated amine units (—NH^+) present in the PANI.[45] The peak observed at the binding energy 531.2 eV is characteristic of O_{1s}, suggesting that oxygen atom is present in "O^{2-} state" in the composite.[46] The XPS spectrum corresponding to Sn energy levels [Figure 3(d)] shows appearance of peaks at the binding energies 487.23 and 495.61 eV, which are assigned to $Sn_{3d}5/2$ and $Sn_{3d}3/2$ states, respectively.[47] The atomic ratio, Sn : O, determined from the area under the Sn and O peaks, is found to be ~1 : 1.98, justifying the stoichiometry of the SnO_2 phase. This ratio slightly differs from theoretical value 1 : 2.

The electrochemical measurements were performed in 1M H_2SO_4 as an electrolyte. The CV was performed on three different electrode materials, pristine SnO_2, pristine PANI, and PANI–SnO_2 nanocomposite in separate experiments. The CVs recorded at different scan rates are depicted in Figure 4(a–c). In the case of pristine SnO_2, the observed CV curves exhibit an

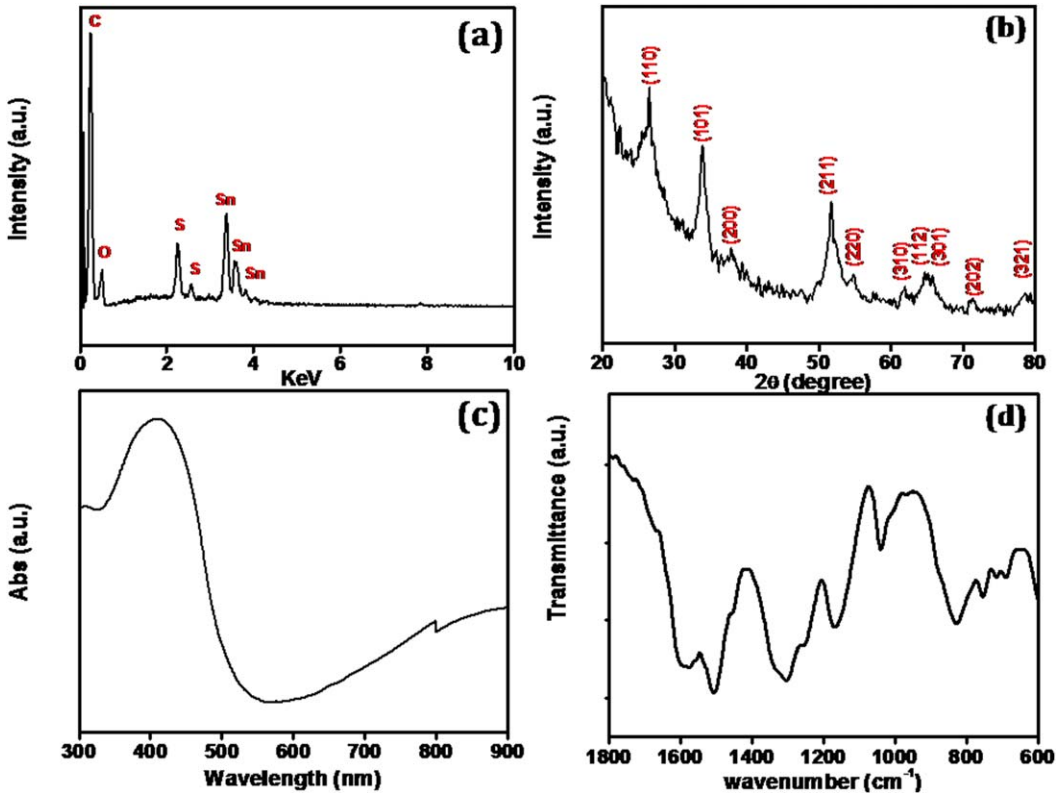

Figure 2. (a) EDAX spectrum (b) XRD spectrum (c) UV–visible spectrum and (b) FTIR spectrum of the PANI–SnO_2 nanocomposite. [Color figure can be viewed in the online issue, which is available at wileyonlinelibrary.com.]

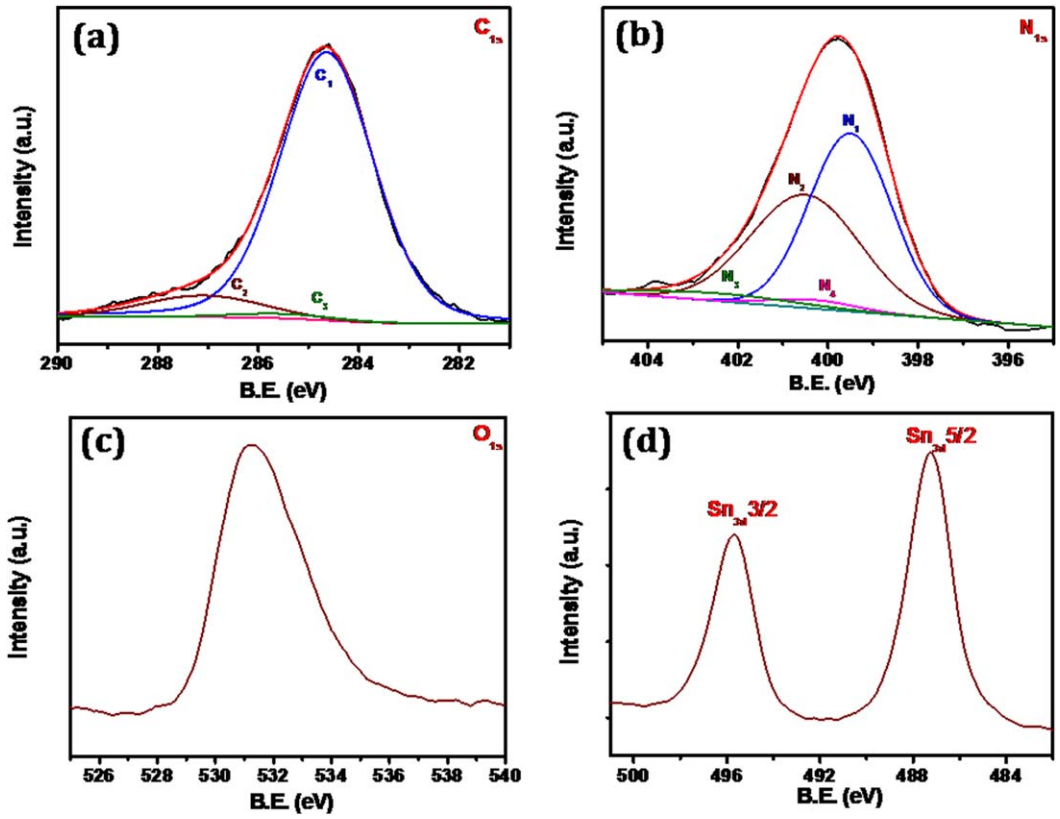

Figure 3. XPS spectra (deconvoluted) of (a) C_{1s}, (b) N_{1s}, (c) O_{1s}, and (d) Sn_{3d} energy levels of the PANI–SnO_2 nanocomposite. [Color figure can be viewed in the online issue, which is available at wileyonlinelibrary.com.]

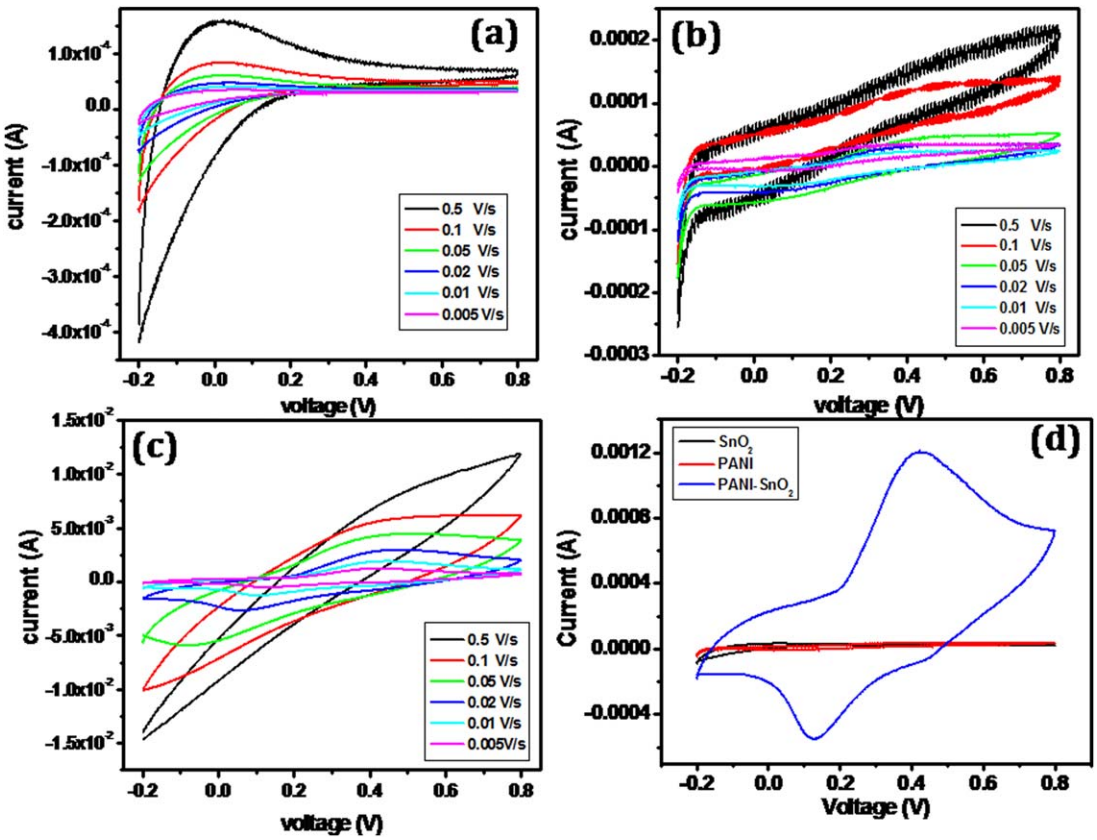

Figure 4. CV curves of different electrodes (a) pristine SnO_2 nanoparticles (b) pristine PANI nanostructures and (c) PANI–SnO_2 nanocomposite, recorded at different scan rates. (d) The CV curves of pristine SnO_2, pristine PANI and PANI–SnO_2 nanocomposite recorded at lowest scan rate of 0.005 V/s. [Color figure can be viewed in the online issue, which is available at wileyonlinelibrary.com.]

anodic peak around −0.05 V. Interestingly, in the case of pristine PANI and PANI–SnO_2 nanocomposite electrodes, the CVs are found to be almost 'rectangular box' type, a characteristic of an ideal supercapacitor with good charge transportation. The observation of significant hysteresis in the CVs of the PANI–SnO_2 nanocomposite is indicative of lower value of the contact resistance. Furthermore, it confirms the pseudocapacitive nature of the electrode material. It is well known that, if the area enclosed by the CV curve increases, the corresponding capacitance value also increases. It is interesting to note that, after the incorporation of the SnO_2 nanoparticles in the PANI nanotubes, the area enclosed by the CV exhibits significant enhancement. The comparative CVs of pristine SnO_2, pristine PANI and PANI–SnO_2 nanocomposite recorded at the scan rate of 0.005V/s are shown in Figure 4(d). The CV area of the PANI–SnO_2 nanocomposite is found to be larger than that of the pristine SnO_2 and PANI films, thus predicting high value of the capacitance i.e. supercapacitive nature of the PANI–SnO_2 nanocomposite.

The current values are observed to be proportional to the scan rate as seen from Figure 5(a). Furthermore, the current values observed in case of PANI–SnO_2 nanocomposite film are higher than those observed for the pristine SnO_2 and PANI films. The higher current values observed for the PANI–SnO_2 nanocomposites can be attributed to better electrical contact between the SnO_2–PANI–ITO phases along with enhanced concentration of the charge carriers. The nearly linear increment in the current value with respect to the scan rate signifies good rate of ability, reversible stability, and fast switching between the oxidation and reduction states on current change. The values of capacitance, estimated at the scan rate 0.005 V/s, are found to be 12.3, 305, and 721 F g^{-1}, for the pristine SnO_2 nanoparticles, pristine PANI nanotubes, and PANI–SnO_2 nanocomposite electrodes, respectively. The increase in the capacitance value of the PANI–SnO_2 nanocomposite is in well agreement with Figure 4(d). The observed supercapacitance value is superior than that of recently reported values for various PANI and SnO_2-based composites like, carbon embedded PANI, graphene/PANI nanofiber composite, SnO_2@C nanocomposite, PANI coated carbon fibbers cloth, RGO/MoO_3/PANI ternary composite films, and PANI/tin oxide hybrid.[10,11,16,19–24] The observed improvement in the capacitance value of the PANI–SnO_2 nanocomposite is attributed to enhancement in the effective surface area of the PANI–SnO_2 nanocomposite. The presence of SnO_2 nanoparticles on the PANI nanotubes increases the surface area of the electrode and, simultaneously helps to decrease the path lengths for the ion exchange between electrode and electrolyte. The possible directions of the electrolyte ions for SnO_2, PANI and PANI–SnO_2 nanocomposite electrode materials are depicted in Scheme 2.

The Figure 5(b) depicts capacitance versus scan rate characteristic of the SnO_2, PANI, and PANI–SnO_2 nanocomposite electrodes. In every case the capacitance value is observed to decrease

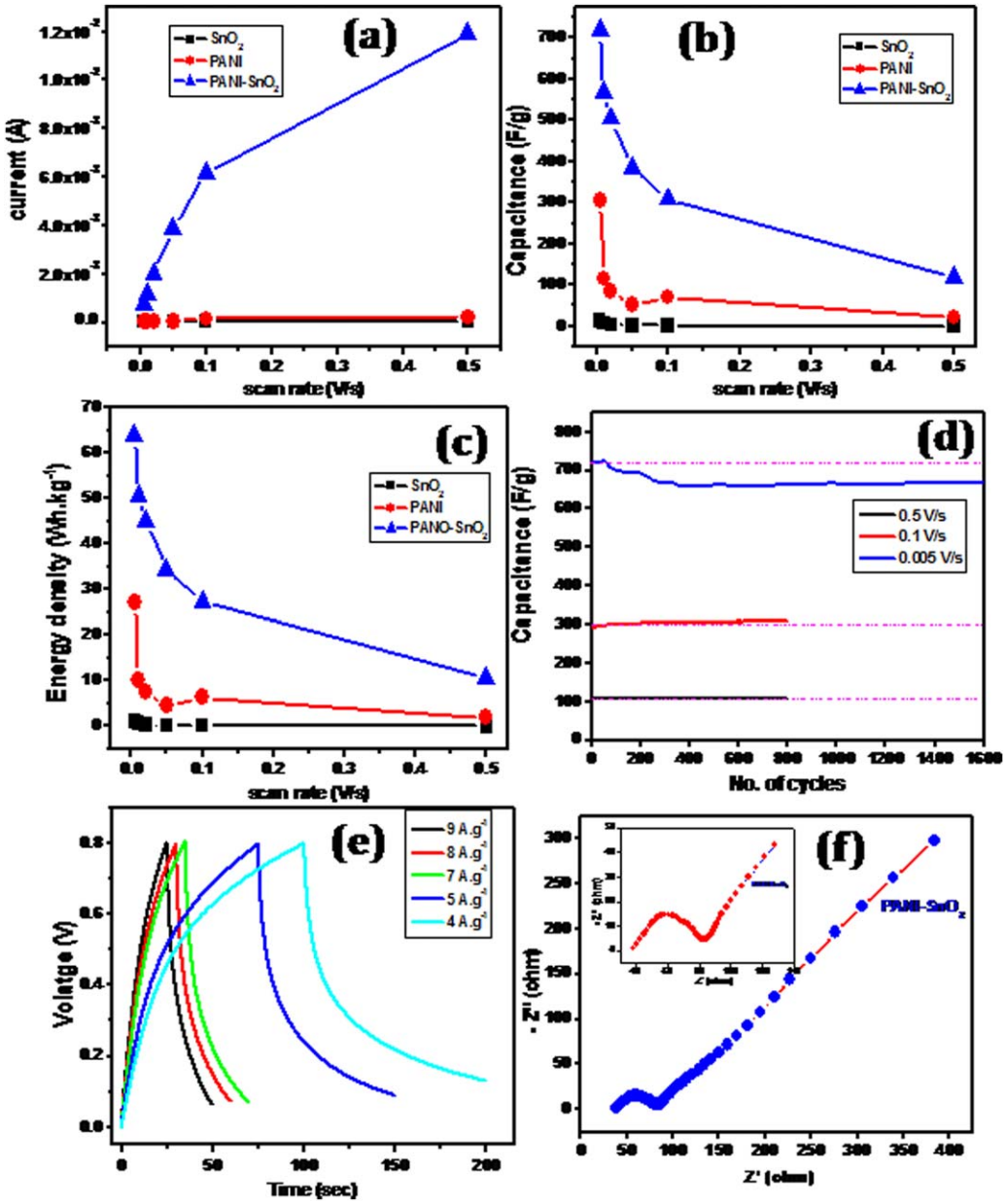

Figure 5. A graph of (a) current versus scan rate (b) capacitance versus scan rate and (c) energy density versus scan rate of SnO_2, PANI and PANI–SnO_2 nanocomposite films. (d) Capacitance stability at scan rate 0.005, 0.1, 0.5 V/s, (e) charging–discharging curve and (f) impedence spectroscopy of PANI–SnO_2 nanocomposite. [Color figure can be viewed in the online issue, which is available at wileyonlinelibrary.com.]

with increase in the scan rate. For the pristine SnO_2 and PANI films, the energy density is calculated to be ~1 and 27 Wh kg^{-1}, respectively. Interestingly, for the PANI–SnO_2 nanocomposite, high value of energy density, ~64 Wh kg^{-1}, is observed. The Figure 5(c) shows a graph of energy density versus scan rate. For the practical application of the super capacitor, stability of the electrode is a key parameter. In the present case, stability of the PANI–SnO_2 nanocomposite electrode has been tested over 1600 CV cycles at the scan rate of 0.005 V/s. As seen from Figure 5(d), the capacitance is observed to be stable over initial 40 cycles, and then it gradually decreases up to 370 cycles, attaining the value ~665 F g^{-1}. Interestingly, the capacitance value over the rest of cycles is seen to be fairly stable up to 1600 cycles. The capacitance stability tests were performed at different scan rates of 0.1 and 0.5 V/s over the duration of 800 cycles. Interestingly, at higher scan rates, the capacitance value is almost stable over the 800 cycles [Figure 5(d)]. The capacitance retention values are found to be 92, 96, and 97% for the scan rates 0.005, 0.1, and 0.5 V/s, respectively.

The GCD is a simple technique to assess applicability of the capacitive material. In case of the PANI–SnO_2 nanocomposite, the charge–discharge cycles have been performed at different current values of 9, 8, 7, 5, and 4 A g^{-1} and are depicted in Figure 5(e). For all current values, the charging–discharging curves exhibit inversion mirror symmetry, exhibiting increasing non-linear behavior with increase in the current density. The

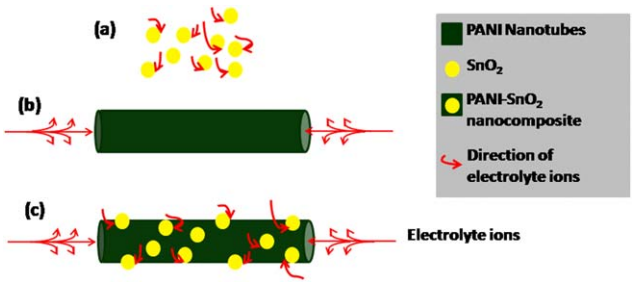

Scheme 2. Plausible directions of electrolyte ions in the (a) SnO_2, (b) PANI, and (c) PANI–SnO_2 nanocomposite electrodes. [Color figure can be viewed in the online issue, which is available at wileyonlinelibrary.com.]

charging–discharging curves show pseudocapacitive behavior with excellent electrochemical performance, which are in good agreement with the observed CV characteristics. The supercapacitance values calculated from the charging–discharging curves are 563, 600, 613, 938, and 1000 F g^{-1}, corresponding to current density values 9, 8, 7, 5, and 4 A g^{-1}, respectively.

Furthermore, impedance spectroscopy is an important tool employed to reveal the electrical characteristics of electrode–electrolyte interface. The Nyquist plot of PANI–SnO_2 nanocomposite electrode recorded in the frequency range from 100 MHz to 1 mHz for is depicted in Figure 5(f). The Nyquist plot shows a semicircular arc in the high frequency region and a straight line at 45° with respect to the real axis in the low frequency region. The diameter of semicircle indicates charge transfer resistance (R_{ct}) of the contact interface between PANI–SnO_2 nanocomposite and electrolyte. In present studies, the value of R_{ct} is observed to 20 ohm. The Wurburg resistance (Z_w) obtained from the slope of straight line at 45° is representative of the ionic charge exchange between electrode and electrolyte. The total resistance, which is combination of the electrolyte resistance, intrinsic resistance of electrode material, and contact resistance, known as series resistance (R_e) can be obtained from the x-intercept of semicircle. From Figure 5(f) the value of R_e is estimated to be ~35 ohm. This implies that the addition of the SnO_2 nanoparticles to the PANI matrix enhances electrical conductivity of the nanocomposite and thus facilitates rapid charge exchange between nanocomposite and electrolyte.

FE investigations of PANI–SnO_2 nanocomposite were performed in a planar diode configuration at base pressure ~1×10^{-8} torr. Figure 6(a) depicts the current density versus applied electric field (J–E) plot of the emitter. Initially, the emission current is observed to increase slowly at lower applied voltages followed by rapid increase, for the same increment in the applied voltage. The exponential nature of J–E plot confirms that the electron emission is due to quantum mechanical tunnelling of electrons as per the Fowler-Nordheim (F-N) theory. The turn on field required to draw an emission current of 1 nA is found to be ~0.73 V/μm, while threshold field required to draw an emission current density of 1 μA/cm^2 is observed to be ~0.90 V/μm, which is lower than the earlier values reported for PANI nanotubes as well as PANI/SnO_2/Sn/MWNT nanocomposite emitters.[30,31] We have observed emission current density of ~1.2 mA/cm^2 at an applied field of 2.6 V/μm. These field values corresponding to the current densities are found to be superior than that reported for conducting PANI and its nanocomposites.[26,28–33] Table I presents the comparison of turn on and threshold field values of various PANI nanostructures and PANI nanocomposites. The superior values of the turn on and threshold fields observed in the present studies are attributed to the enhanced electrical properties of the PANI–SnO_2 nanocomposite (as discussed in earlier section), in addition to their nanometric dimensions (offering high aspect ratio).

The field emission J–E was further analyzed by using the F-N equation:[33]

$$J = \lambda_M a\left(\beta^2 E^2/\varphi\right)\ \exp\ \left(-b\varphi^{3/2} v_F/\beta E\right)$$

where, J is the emission current density at applied average electric field E, a (1.54×10^{-6} A eV V^{-2}) and b (6.83 V $eV^{-3/2}$ nm^{-1}) are constants, λ_M is macroscopic pre-exponential correction factor, v_F (correction factor) is a particular value of the principal Schottky-Nordheim barrier function v, φ is the work function and β is field enhancement factor. The graph of $\ln(J/E^2)$ versus $1/E$ known as the Fowler-Nordheim (F-N) plot, is depicted as inset of Figure 6(a).

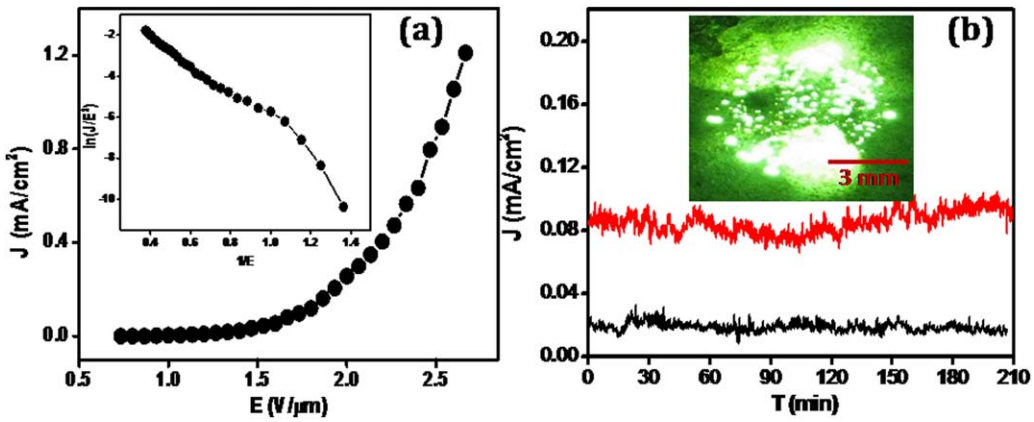

Figure 6. The FE characteristics of the PANI–SnO_2 nanocomposite emitter (a) The emission currents density versus applied electric field ($J-E$) plot, with F-N plot as the inset and (b)emission current versus time ($I-t$ plot) plot, with FE image as the inset. [Color figure can be viewed in the online issue, which is available at wileyonlinelibrary.com.]

Table I. Comparison of the Turn on and Threshold Field Values of Different Emitters Due to Conducting Polymers and Their Composites

Material	Turn on field for 1 nA	Threshold field for 1 μA/cm^2	Threshold field for 10 μA/cm^2	Reference
PANI-SnO_2 nanotube composite	0.73 V/μm	0.9 V/μm	1.2 V/μm	Present studies
Aligned PANI nanofibers	-	-	5-6 V/μm	26
1% DWNT-PANI	-	2.0 V/μm	-	28
1% SWNT-PANI/CSA	-	-	2.3 V/μm	
1% SWNT-PANI	3.1 V/μm for 5 μA/cm^2	-		
0.3% SWNT-PANI	2.5 V/μm for 1.5 μA/cm^2	-		
0.5% DWNT-PANI	2.3 V/μm for 1.5 μA/cm^2	-		
PANI/MWNT	-	-	2.12 V/μm	29
PANI/SnO_2/Sn/MWNT	-	1.8 V/μm	-	30
PANI nanotube	1.3 V/μm	1.55 V/μm	1.7 V/μm	31
Aligned PANI nanofibers	1.6 V/μm	-	2.85 V/μm	32
Aligned PANI nanotubes	2.4 V/μm	-	3.95 V/μm	
PANI nanopetals	1.6 V/μm	2.3 V/μm	3.6 V/μm	33
PANI nanocrystals	1.6 V/μm	1.8 V/μm	1.9 V/μm	

The non-linear behavior of the F-N plot is indicative of semiconducting nature of the emitter. Furthermore, in case of a "multi-tip" emitter (an assembly of nanostructures deposited in thin film form) various factors, such as electric field screening effect, band bending, band penetration etc, do affect the nature of F-N plot. Many researchers have estimated the value of field enhancement factor (β) from slope of the F-N plot. However, it has been observed that for a multi-tip emitter the value of β thus obtained is 'over estimated'. If one tries to estimate the value of the local field ($E_{local} = \beta E_{av}$) using the β value obtained from the F-N equation, then the value of E_{local} is found to be very high, an order of magnitude higher than that required for FE, and thus seems to be "unphysical." Hence, in the present studies we have not estimated the value of β.

Along with the FE characteristics, stability of the field emitter is also one of the important parameters from the application point of view. In the present case, the emission stability has been investigated over duration of more than 3 h at preset values of ~0.02 and ~0.1 mA/cm^2 and the corresponding emission current versus time ($I - t$) plots are depicted in Figure 6(b). In both the cases, the noise, i.e., fluctuations in the emission current are found to be within $\pm$ 10% of the average value. The "spike" like fluctuations are attributed to the adsorption–desorption of the residual gas species on the emitter surface. The FE image recorded at an applied field of 2.6 V/μm is depicted as the inset of Figure 6(b). The bright FE images comprised of large number of tiny spots suggests that the emission is from the PANI–nanotubes as well as from small clusters of SnO_2 nanoparticles sitting on the polymer nanotubes.

CONCLUSIONS

A Simple two step chemical route is employed to synthesize PANI–SnO_2 nanocomposite. The as-synthesized PANI–SnO_2 nanocomposite has been is characterized by various techniques, including SEM, TEM, XRD, FTIR, and XPS before supercapacitive measurements. The supercapacitance value of the PANI–SnO_2 nanocomposite is observed to be higher, in contrast to the pristine SnO_2 and PANI electrodes. Interestingly, supercapacitance of 721 F g^{-1} is observed for PANI–SnO_2 nanocomposite at the scan rate of 0.005 V/s, with high energy density of 64 Wh kg^{-1}. The retention in the capacitance value is observed to be 92% at this scan rate and it increases to 96.68% and 97.6% at higher scan rates 0.1 and 0.5 V/s, respectively. The charge–discharge characteristics reveal pseudocapacitive nature of the PANI–SnO_2 nanocomposite. The observed values of charge transfer and series resistances, estimated from the Nyquist plot are found to be low. The FE characteristics of the PANI–SnO_2 nanocomposite emitter are found superior to the earlier reports. Furthermore the emitter exhibits good emission stability at ~0.02 and ~0.1 mA/cm^2 over duration of more than 3 h. The enhancement in the capacitance value and superior FE behavior exhibited by the PANI–SnO_2 nanocomposite are attributed to the synergic effect of SnO_2 nanoparticles and PANI nanotubes.

ACKNOWLEDGMENTS

Dr. S. S. Patil acknowledge BARC for financial assistance. Authors are sincerely thankful to Prof. S. R. Jadkar for the impedance measurements. The field emission work is carried out as part of CNQS program.

REFERENCES

1. Bhadra, S.; Khastgir, D.; Singha, N. K.; Lee J. H. *Prog. Polym. Sci.* **2009**, *34*, 783.
2. Tran, H. D.; D'Arcy, J. M.; Wang, Y.; Beltramo, P. J.; Strong, V. A.; Kaner, R. B. *J. Mater. Chem.* **2011**, *21*, 3534.
3. Ciric-Marjanovic, G. *Synth. Met.* **2013**, *177*, 1.
4. Wang, G.; Zhang, L.; Zhang, J. *Chem. Soc. Rev.* **2012**, *41*, 797.
5. Fan, H.; Wang, H.; Zhao, N.; Zhang, X.; Xu, J. *J. Mater. Chem.* **2012**, *22*, 2774.

6. Miao, Y.-E.; Fan, W.; Chen, D.; Liu, T. *ACS Appl. Mater. Inter.* **2013**, *5*, 4423.
7. Shaikh, S. F.; Lim, J.-Y.; Mane, R. S.; Zate, M. K.; Han, S.-H.; Joo, O.-S. *J. Appl. Poly. Sci.* **2013**, *128*, 3660.
8. Wang, K.; Huang, J.; Wei, Z. *J. Phys. Chem. C* **2010**, *114*, 8062.
9. Rakhi, R. B.; Chen, W.; Alshareef, H. N. *J. Mater. Chem.* **2012**, *22*, 5177.
10. Kovalenko, I.; Bucknall, D. G.; Yushin, G. *Adv. Funct. Mater.* **2010**, *20*, 3979.
11. Cheng, Q.; Tang, J.; Ma, J.; Zhang, H.; Shinya, N.; Qin, L.-C. *J. Phys. Chem. C* **2011**, *115*, 23584.
12. Ge, J.; Cheng, G.; Chen L. *Nanoscale* **2011**, *3*, 3084.
13. He, S.; Hu, X.; Chen, S.; Hu, H.; Hanif, M.; Hou, H. *J. Mater. Chem.* **2012**, *22*, 5114.
14. Kumar, N. A.; Choi, H.-J.; Shin, Y. R.; Chang, D. W.; Dai, L.; Baek, J.-B. *ACS nano* **2012**, *6*, 1715.
15. Mao, L.; Zhang, K.; On Chan, H. S.; Wu, J. *J. Mater. Chem.* **2012**, *22*, 80.
16. Wu, Q.; Xu, Y.; Yao, Z.; Liu, A.; Shi, G. *ACS nano.* **2010**, *4*, 1963.
17. Li, L.; Raji, A.-R.O.; Fei, H.; Yang, Y.; Samuel, E. L. G.; Tour, J. M. *ACS Appl. Mater. Inter.* **2013**, *5*, 6622.
18. Rakhi, R. B.; Chen, W.; Cha, D.; Alshareef, H. N. *J. Mater. Chem.* **2011**, *21*, 16197.
19. Selvan, R. K.; Perelshtein, I.; Perkas, N.; Gedanken, A. *J. Phys. Chem. C* **2008**, *112*, 1825.
20. Xia, X.; Hao, Q.; Lei, W.; Wang, W.; Wang, H.; Wang, X. *J. Mater. Chem.* **2012**, *22*, 8314.
21. Wang, L.; Chen, L.; Yan, B.; Wang, C.; Zhu, F.; Jiang, X.; Chaob, Y.; Yang, G. *J. Mater. Chem. A* **2014**, *2*, 8334.
22. Zhu, Y.; Liu, E.; Luo, Z.; Hu, T.; Liu, T.; Li, Z.; Zhao, Q. *Electrochem. Acta* **2014**, *118*, 106.
23. Li, X.; Chai, Y.; Zhang, H.; Wang, G.; Feng, X. *Electrochim. Acta.* **2012**, *85*, 9.
24. Hu, Z.-A.; Xie, Y.-L.; Wang, Y.-X.; Mo, L.-P.; Yang, Y.-Y.; Zhang, Z.-Y. *Mater. Chem. Phys.* **2009**, *114*, 990.
25. Amaratunga, G. A. J.; Musa, I.; Munindrasdasa, D. A. I. *Nature* **1998**, *395*, 362.
26. Wang, C.; Wang, Z.; Li, M.; Li, H. *Chem. Phys. Lett.* **2001**, *341*, 431.
27. Kim, B. H.; Park, D. H.; Joo, J.; Yu, S. G.; Lee, S. H. *Synth. Met.* **2005**, *150*, 279.
28. Nair, R.; Premlal, B.; Das, A.; Sood, A. K. *Solid State Commun.* **2009**, *149*, 150.
29. Rakhi, R. B.; Sethupathi, K.; Ramaprabhu, S. *Appl. Surf. Sci.* **2008**, *254*, 6770.
30. Rakhi, R. B.; Sethupathi, K.; Ramaprabhu, S. *J. Exp. Nanosci.* **2009**, *4*, 67.
31. Patil, S. S.; Koiry, S. P.; Aswal, D. K.; Koinkar, P. M.; Murakami, R.-C.; More, M. A. *J. Electrochem. Soc.* **2011**, *158*, E63.
32. Patil, S. S.; Koiry, S. P.; Veerender, P.; Aswal, D. K.; Gupta, S. K.; Joag, D. S.; More, M. A. *RSC Adv.* **2012**, *2*, 5822.
33. Patil, S. S.; Koiry, S. P.; Aswal, D. K.; Koinkar, P.; More, M. A. *J. Electrochem. Soc.* **2013**, *160*, D543.
34. Khuspe, G. D.; Chougule, M. A.; Navale, S. T.; Pawar, S. A.; Patil, V. B. *Ceram. Int.* **2014**, *40*, 4267.
35. Manivel, P.; Ramakrishnan, S.; Nikhil, N., Kothurkar, K.; Balamurugan, A.; Ponpandian, N.; Mangalaraj, D.; Viswanathan, C. *Mater. Res. Bull.* **2013**, *48*, 640.
36. Gu, F.; Fen Wang, S.; Feng Song, C.; Kai Lü, M.; Xin Qi, Y.; Jun Zhou, G. *Chem. Phys. Lett.* **2003**, *372*, 451.
37. Trchová, M.; Šeděnková, I.; Konyushenko, E. N.; Stejskal, J.; Holler, P.; Ćirić-Marjanović, G. *J. Phys. Chem. B* **2006**, *110*, 9461.
38. Wei, D.; Kvarnström, C.; Lindfors, T.; Ivaska, A. *Electrochem. Commun.* **2006**, *8*, 1563.
39. Zhang, L.; Peng, H.; Sui, J.; Kilmartin, P. A.; Travas-Sejdic, J. *Curr. Appl. Phys.* **2008**, *8*, 312.
40. Zhang, L.; Zujovic, Z. D.; Peng, H.; Bowmaker, G. A.; Kilmartin, P. A.; Travas-Sejdic, J. *Macromolecules* **2008**, *41*, 8877.
41. Zhang, L.; Wan, M. *Nanotechnology* **2002**, *13*, 750.
42. Ma, X.; Wang, M.; Li, G.; Chen, H.; Bai, R. *Mater. Chem. Phys.* **2006**, *98*, 241.
43. Min, S.; Wang, F.; Han, Y. *J. Mater. Sci.* **2007**, *42*, 9966.
44. Qaiser, A. A.; Hyland, M. M.; Patterson, D. A. *J. Phys. Chem. B.* **2011**, *115*, 1652.
45. Zou, B.-X.; Liang, Y.; Liu, X.-X.; Diamond, D.; Lau, K.-T. *J. Power Sources.* **2011**, *196*, 4842.
46. Davar, F.; Salavati-Niasari, M.; Fereshteh, Z. *J. Alloys Comp.* **2010**, *496*, 638.
47. Liang, R.; Cao, H.; Qian, D.; Zhang, J.; Qu, M. *J. Mater. Chem.* **2011**, *21*, 17654.